

Article

# UAV Dynamic Non-Terrestrial Transmission Channel Analysis Based on SSCM-RT Model

Jinsheng Yang <sup>1</sup>, Huan Xi <sup>1,\*</sup>, Zhou Pan <sup>2</sup> and Ying Zhou <sup>2</sup><sup>1</sup> School of Microelectronics, Tianjin University, Tianjin 300072, China; jsyang@tju.edu.cn<sup>2</sup> Tianjin Navigation Instrument Research Institute, Tianjin 300131, China; panli\_an@163.com (Z.P.); 13911169155@163.com (Y.Z.)

\* Correspondence: xh\_623840602@163.com; Tel.: +86-1320-752-25-12

**Abstract:** Unmanned Aerial Vehicles (UAVs) have become crucial components of building air-ground integrated networks for sixth-generation mobile communications. UAV-related technology has advanced quickly in both military and civilian contexts. Problems with long-distance and dynamic communication need to be fixed in the non-terrestrial transmission channels of high-altitude UAVs. For long-distance UAV dynamic non-terrestrial transmission channel modeling, a spatial statistical channel model–ray tracing (SSCM-RT) hybrid channel model is proposed and verified, and SSCM-RT channel simulations incorporating spatial consistency analysis are carried out to realize the description of the communication process in the dynamic scenario of the non-terrestrial transmission in symmetric and asymmetric situations. The SSCM-RT model can output channel state information continuously, which is helpful for the quantitative description and characterization of the UAV channel in practical settings.

**Keywords:** UAV; millimeter wave; non-terrestrial transmission; channel modeling; spatial consistency



**Citation:** Yang, J.; Xi, H.; Pan, Z.; Zhou, Y. UAV Dynamic Non-Terrestrial Transmission Channel Analysis Based on SSCM-RT Model. *Symmetry* **2023**, *15*, 1955. <https://doi.org/10.3390/sym15101955>

Academic Editor: Sergei D. Odintsov

Received: 19 September 2023

Revised: 19 October 2023

Accepted: 20 October 2023

Published: 23 October 2023



**Copyright:** © 2023 by the authors. Licensee MDPI, Basel, Switzerland. This article is an open access article distributed under the terms and conditions of the Creative Commons Attribution (CC BY) license (<https://creativecommons.org/licenses/by/4.0/>).

## 1. Introduction

The fifth-generation (5G) wireless communication technology has developed quickly and has been used continually as a result of the ongoing advancement of the global information process. As shown in Figure 1, all kinds of UAVs have become an important component and effective supplement to realize the 6G air–space–ground–sea integrated communication system [1] and have become an important part of building a space–air–ground integrated network (SAGIN) [2]. Full-spectrum resources, such as sub-6 GHz, millimeter wave (mmWave), terahertz, and optical bands, will be increasingly explored [3]. To fulfill the increased demand for higher data rates, millimeter wave bands and broadband wireless communication links both offer new facilities for 5G mobile communication networks [4].

Due to the substantial propagation losses that millimeter waves experience due to long-distance communication, these losses are typically reduced by using highly directed antennas or antenna arrays [5,6]. Omnidirectional antennas perform better in terms of communication performance during movement from the perspective of UAV control, while directional antennas struggle [7]. To better satisfy the demands of long-distance communication, Multiple-Input Multiple-Output (MIMO) antenna arrays can be used. Multiple antennas in a MIMO system can be used in many ways to maximize efficiency. MIMO antenna arrays can increase channel reliability and channel capacity [8]. Spatial multiplexing (SM) and beamforming (BF) are the most popular of these [9].

Low-altitude and high-altitude UAVs can cooperate to complete challenging targeting missions. In complex battlefield scenarios with potent electronic jamming and anti-aircraft firepower, as well as those that include non-terrestrial network (NTN) communication issues, micro UAVs have clear advantages such as indestructibility, low cost, and function distribution [10,11]. NTNs can provide us with multicast opportunities over very large areas as well as can serve users even in remote areas or during times of natural calamities [12].

It is suggested that NTN can conduct high-capacity millimeter wave transmission in the 3GPP specification, which calls for enormous bandwidth and can achieve high-speed connection using high-directional antennas [13]. Meanwhile, high-altitude UAVs have broader coverage than low-altitude UAVs and have lower path loss than high-altitude platforms. This mainly depends on the altitude of the flights. Therefore, the research into the communication channel characteristics of high-altitude UAVs and the non-terrestrial network transmission characteristics of UAV relays is relevant to the national military and security.

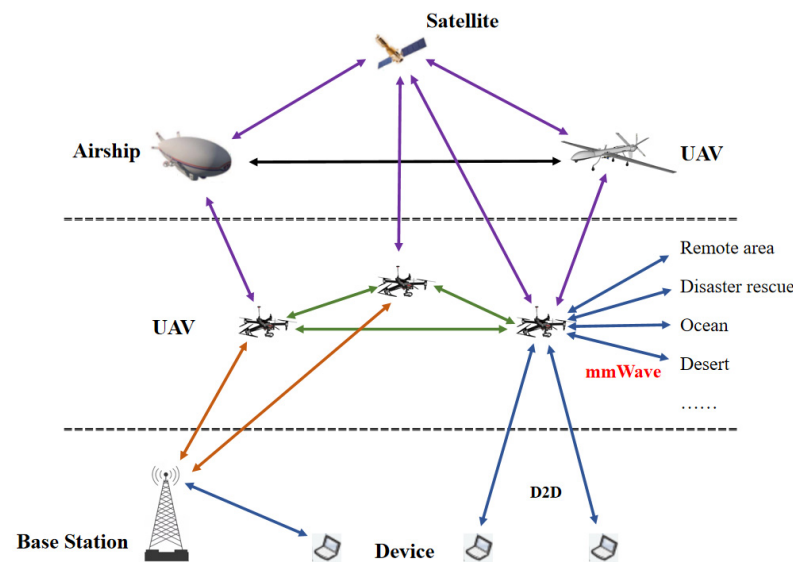


**Figure 1.** Millimeter-wave band UAV application scenarios.

Statistical, deterministic, and semi-deterministic models are the primary types of wireless channel models used today. A vast number of observed data are used in the statistical modeling method to determine the channel impulse response, which is then used to generalize the channel's statistical properties and empirical formula to other scenarios with comparable structural elements. Common statistical channel models such as the spatial statistical channel model have trouble adequately describing the conditions of dynamic communication channels [9]. The deterministic model is based on the electromagnetic wave propagation mechanism, predicts and analyzes the wireless channel characteristics by particular environmental conditions, but has significant computational complexity on air attenuation. The diffusion angle of some scattering components usually does not affect end-to-end channel transmission, but ray-tracing algorithms still take it into account. The complexity can be reduced using the semi-deterministic model. However, there is a significant error in simulating the propagation's environmental conditions.

The fundamental tenet of the ray-tracing (RT) technique is that the ray approximation of geometrical optics can be used to study electromagnetic wave rays when their wavelength is sufficiently small in comparison to the size of the building. The emitting source is also considered a point source, and the propagation from each source point to the field point is determined from the ray. After integrating each ray's propagation, antenna information at the receiver, and vector superposition of each arriving ray, calculations such as line–plane intersection are utilized to explain the channel propagation characteristics.

Chen et al. [14] examined an indoor Geometry-based Stochastic Channel Model-Ray Tracing (GSCM-RT) hybrid channel model, which does not account for long-distance path loss and air attenuation. Luo et al. [15] created a hybrid near–far field channel model for massive reconfigurable-intelligent-surface-assisted communication by introducing a weighting factor. The theoretical foundation for our study is provided by the above references.

In this study, SSCM-RT channel modeling and simulation are used to examine the UAV dynamic non-terrestrial transmission channel with a focus on the issues with long-distance

communication and dynamic scenario challenges. The main research contents of this paper are as follows:

- A long-distance non-terrestrial transmission channel model for UAVs is established. The channel parameters chosen for the simulation are based on the spatial statistical channel model. To confirm the validity of the SSCM-RT channel model, the path loss simulation results are compared with those from other models.
- The relative motion of the UAVs is simulated using various motion models in symmetric and asymmetric scenarios, and the spatial consistency's impact on the channel is examined. The channel characteristics of several motion models are simulated to further confirm the reliability of the SSCM-RT model.

The remainder of this study is organized as follows. Section 2 introduces the channel fading model parameters and the concept of spatial consistency. Section 3 establishes a long-distance non-terrestrial transmission channel model for UAVs and analyzes the non-terrestrial transmission channel using the SSCM-RT model. Section 4 introduces spatial consistency using various motion models and simulates dynamic scenarios using the SSCM-RT model. Section 5 provides a conclusion.

## 2. Theoretical Background

The channel fading model parameters and the concept of spatial consistency are introduced in this section, which provides a theoretical basis for the research of this paper.

### 2.1. Channel Fading Model Parameters

Radio waves can be classified according to the fading type as large-scale fading and small-scale fading, depending on the interval at which the received signal field strength changes. Signals will encounter large-scale and small-scale fading throughout the real scene propagation processes. Large-scale fading typically impacts the wireless system's ability to provide network coverage, while small-scale fading impacts the communication system's quality [16–18].

Path loss and shadow fading are used to characterize the properties of large-scale fading. Large-scale average path loss is used to assess the average fading of the signal between the transmitter and receiver and is defined as the difference between the effective transmit power and the average received power. For shadow fading, when radio signals are transmitted in channels at mesoscale distances, obstructions such as terrain undulations or tall building groups can cause the formation of a shadow area behind the obstruction, leading to erratic changes in the average power of the received signal. It fades in a manner that roughly corresponds to a lognormal distribution [19].

When a radio signal rapidly changes in amplitude, phase, or multipath delay over a short period of time or space (a few wavelengths), it is referred to as small-scale fading. It is caused by the same transmission signal traveling along different paths, and the signals arriving at the receiver at different moments (or phases) are superimposed on each other. The signals that travel along these various paths include direct path and multipath signals produced by scatterers, such as reflection, diffraction, and scattering. Small-scale channel modeling primarily takes the modeling of temporal dispersion parameters, frequency dispersion parameters, and spatial dispersion characteristics into account [20].

The symbols and descriptions of channel parameters are shown in Appendix A.

According to the table in Appendix A, the omnidirectional received power can be described as

$$P_{r-omni} = \sum_{i,j} \sum_{k,m} P_r(AZ_{TX,i}, EL_{TX,j}, AZ_{RX,k}, EL_{RX,m}) \cdot d_{T-R}, \quad (1)$$

where  $i, j, k, m$  denote unique pointing directions indices in azimuth and elevation at the TX and RX, respectively.  $AZ_{TX,i}, EL_{TX,j}, AZ_{RX,k}, EL_{RX,m}$  represent the TX azimuth and elevation angles, and the RX azimuth and elevation angles, respectively [21].

Path loss can be described as

$$PL[\text{dB}] = FSPL[\text{dB}] + 10\lg(d/d_0) + AT[\text{dB}] + X_\sigma[\text{dB}], \quad (2)$$

where  $FSPL$  implies free space path loss,  $AT$  is related to the attenuation factor which includes the collective attenuation effects of dry air (including oxygen), water vapor, rain, and haze.  $X_\sigma$  is a zero-mean Gaussian random variable with a standard deviation  $\sigma$  in dB.  $d_0$  signifies the free space reference distance, and should not exceed 5 m to guarantee free space propagation [22].

According to the Friis transmission equation, free space path loss can be described as

$$FSPL[\text{dB}] = -32.44 - 20\lg d_{T-R} - 20\lg f, \quad (3)$$

the unit of  $d_{T-R}$  is km, the unit of  $f$  is MHz [23].

From another point of view, the directional path loss can be written as

$$PL = P_{TX} + G_{TX} + G_{RX} - P_r. \quad (4)$$

In addition, the relationship between time delay and T-R separation distance for Line of Sight (LOS) can be described as

$$\tau = \frac{d_{T-R}}{c}, \quad (5)$$

where  $c$  represents the electromagnetic wave propagation speed. Therefore, in the presence of multipath components, each multipath component has a slightly larger time delay than the direct path.

The open-source millimeter wave channel modeling software simulator (NYUSIM Version 3.1) is used in this study to obtain the SSCM channel parameters [24].

At a T-R separation of 2000 m, Figure 2 depicts the frequency dependence of path loss using the statistical channel model. When the frequency is below 50 GHz, the relationship between the path loss and frequency is linear; however, as the frequency grows, the path loss increases quickly. To prevent severe and quick channel fading, the high-altitude UAV's frequency choice should ideally not exceed 50 GHz. The path loss exponent exhibits a similar trend, as illustrated in Figure 3. These are mainly related to atmospheric attenuation. Due to the absorption characteristics of the atmosphere, oxygen, and water vapor in the air absorb electromagnetic waves more severely, with an absorption peak near the frequency of 60 GHz.

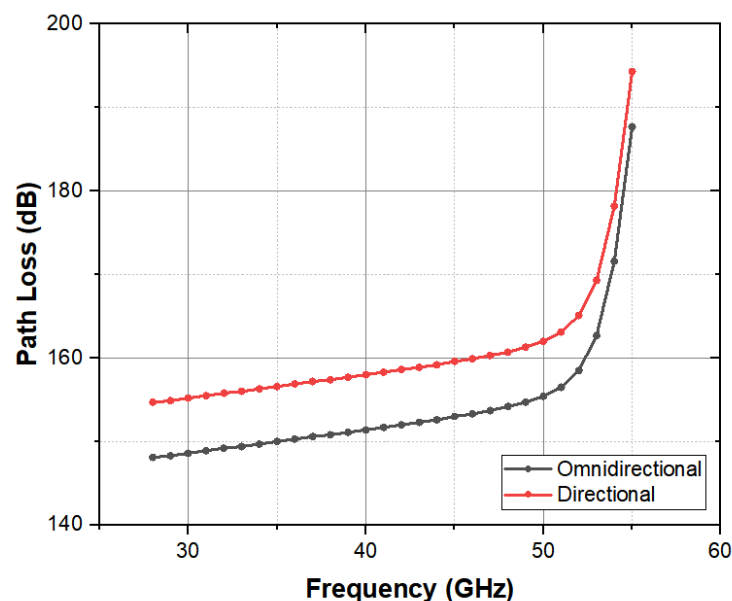
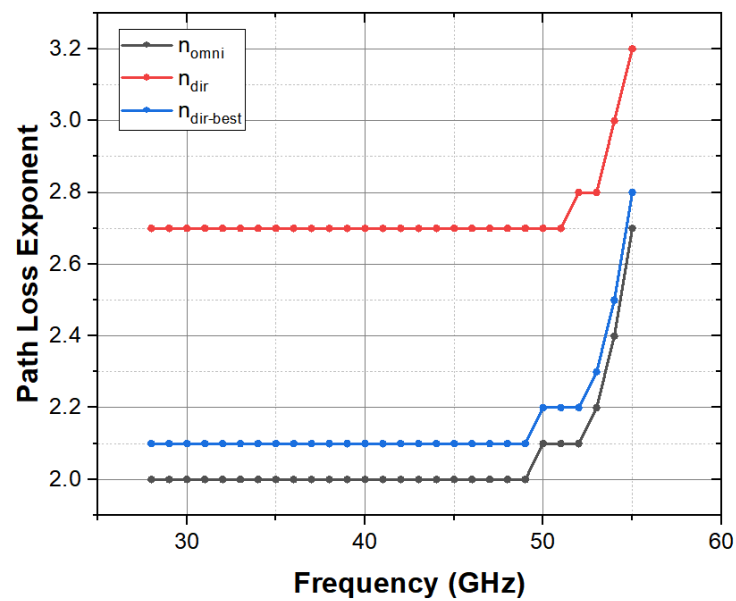


Figure 2. The frequency dependence of path loss by using the statistical channel model.



**Figure 3.** The relationship of path loss exponent and frequency by using the statistical channel model.

### 2.2. Spatial Consistency

Spatial consistency is an essential characteristic of time-varying channels for outdoor scenes, specifically the characteristic that the channel parameters vary continuously over time and space, and the study of channels including spatial consistency can improve the simulation's realism.

The 3GPP TR38.901 file contains the channel correlation matrix information that is used to choose the correlation distance for various scenario contexts in the spatial consistency simulation. Correlation distance determines the length of a channel segment. Within the correlation distance range, large-scale parameters are considered spatially correlated during the UAV movement. Correlation distance for spatial consistency is shown in Table 1.

**Table 1.** Correlation distance for spatial consistency.

Correlation Distance (m)	Rural Macro			Urban Micro			Urban Macro			Indoor
	LOS	NLOS	O2I	LOS	NLOS	O2I	LOS	NLOS	O2I	
Cluster and ray specific random variables	50	60	15	12	15	15	40	50	15	10
LOS/NLOS state		60			50			50		10
Indoor/Outdoor state		50			50			50		N/A

## 3. SSCM-RT Channel Model

In this research, a long-distance 3D hybrid channel model for UAVs is suggested and simulated based on the comparison of several modeling methods. This model combines the spatial statistical channel model (SSCM) and ray tracing (RT).

### 3.1. Modeling Scenario Characterization

The SSCM-RT model divides long-distance propagation into two parts, using the ray tracing model for deterministic modeling in the portion of the propagation distance close to the receiver and the spatial statistical channel model in the portion of the propagation distance far from the receiver. The electromagnetic wave's polarization angle may shift when the wavelength is close to the diameter of a raindrop, complicating the calculation. In the long-distance transmission process, the spatial statistical channel model can be used to calculate the influence of atmospheric attenuation on the channel more simply and reduce the complexity of the ray tracing technique computation in this section of the

attenuation. The ray tracing model can guarantee a more precise characterization of the multipath component of the dynamic channel at close range. The specific implementation and guiding concepts of SSCM-RT channel modeling are as follows:

In this section, assume that the low-altitude UAV flies at a constant altitude and makes a circular motion with a radius of 100 m. Assume that the high-altitude UAV is stationary relative to its circular motion, and the projection point to the plane where the low-altitude UAV is located is at the center of the circle, as shown in Figure 4. The channel is divided into two parts of the propagation process. One is the long-distance propagation part. This mode of motion presents symmetry. The use of statistical channel modeling can better describe the environmental impact such as atmospheric attenuation, and set the distance of this part as  $d_1$ . The other is the close-range propagation part. The model, morphology, and motion of the UAV will have a certain influence. Therefore, the deterministic modeling method can obtain more accurate dynamic data, and set the distance of this part as  $d_2$ .

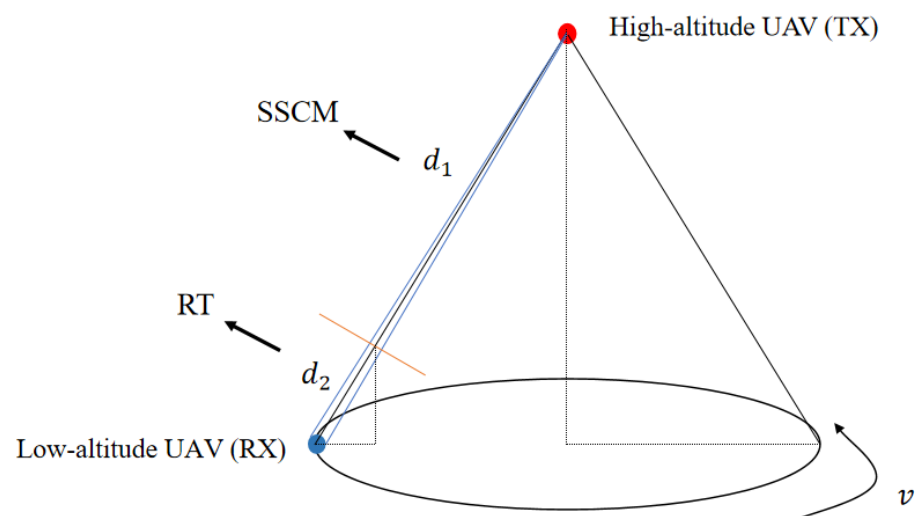


**Figure 4.** Long-distance UAVs communication scenario of SSCM-RT. The red point represents a high-altitude UAV that carries TX; the blue point represents a low-altitude UAV that carries RX.

Five channel modeling effects can be offered for comparison in this scenario, matching the statistical channel parameter values, including the SSCM model only, the RT model only, the 3GPP-GSCM model, the simple prorate model, and the SSCM-RT hybrid model proposed in this study. The traditional two-path ground reflection model is not applicable for inter-UAV communication and it is challenging to cancel the other multipath components in the actual air-to-ground channel with small errors; thus, no comparison is made in this paper.

The 3GPP-GSCM model is a traditional geometry-based random channel model. In this paper, the time-varying channel model constructed by 3GPP TR38.901 is used as a comparison.

Simple prorate modeling is based on the cascade channel modeling method from the reference [15]. Path loss in this reference can be written as

$$\begin{aligned}
 PL(CAS) &= \omega P_L(\text{far-field}) + (1 - \omega) P_L(\text{near-field}) \\
 &= \frac{c^2}{\left(\frac{4\pi}{\lambda}\right)^2 d_1^2 d_2^2} e^{-j\frac{2\pi}{\lambda}(d_1+d_2)} + \frac{c^2}{\left(\frac{4\pi}{\lambda}\right)^2 (d_1+d_2)^2} e^{-j\frac{2\pi}{\lambda}(d_1+d_2)}, \quad (6)
 \end{aligned}$$

where  $\omega = \frac{G_{far}}{G_{near}+G_{far}}$ ,  $G_{far}$  and  $G_{near}$  are the total gain in the far-field and the total gain in the near-field, respectively. It follows that the result is related to  $\frac{d_1}{d_2}$ . This provides the theoretical basis for the cascade channel system and also provides the theoretical basis and feasibility support for the SSCM-RT channel modeling reference in this paper.

The SSCM-RT hybrid channel model proposed in this paper combines the advantages of the statistical channel modeling method and ray tracing method. Taking path loss as an example, when assuming that both path  $d_1$  and  $d_2$  of the channel are known, the path loss in segment  $d_1$  can be written as

$$P_{L-SSCM}(d_1)[\text{dB}] = P_{L-SSCM}(d_1 + d_2)[\text{dB}] - P_{L-SSCM}(d_2)[\text{dB}]. \quad (7)$$

The total path loss can be written as

$$\begin{aligned} PL[\text{dB}] &= P_{L-SSCM}(d_1)[\text{dB}] + P_{L-RT}(d_2)[\text{dB}] \\ &= P_{L-SSCM}(d_1 + d_2)[\text{dB}] - P_{L-SSCM}(d_2)[\text{dB}] + P_{L-RT}(d_2)[\text{dB}] \\ &= 20 \lg \frac{1}{\frac{d_1}{d_2} + 1} + 10n \cdot \lg \left( \frac{d_1}{d_2} + 1 \right) + X_\sigma(d_1 + d_2) - X_\sigma(d_2) + P_{L-RT}(d_2)[\text{dB}] \quad (8) \\ &= 10(n - 2) \lg \left( \frac{d_1}{d_2} + 1 \right) + X_\sigma(d_1 + d_2) - X_\sigma(d_2) + P_{L-RT}(d_2)[\text{dB}]. \end{aligned}$$

It is consistent with the definition and range of PLE. According to the simulation results in Section 2.1, the first part of Equation (8) can be calculated by bringing in the corresponding value of  $n$ .  $X_\sigma$  depends on the variance  $\sigma$  and the relationship of  $d_1$  and  $d_2$ .  $P_{L-RT}(d_2)$  is calculated by an equivalent RT simulation. This only applies to the case of two segments.  $X_\sigma(d_1 + d_2)$  and  $X_\sigma(d_2)$  obey the same zero-mean Gaussian random variable. This implies that the estimated PL's variance has not doubled.

According to the results in the reference [17], electromagnetic waves transmitted over long distances can be approximated as parallel line propagation if the free space propagation model is used as a reference. This also demonstrates the validity of the equivalent RT part of the simulation in this SSCM-RT model.

The GSCM-RT hybrid model proposed in reference [14] also provides a theoretical basis for this paper. While the long-distance path loss in the scenario of this paper is non-negligible, the results of the statistical channel model have greater practicality compared with reference [14].

### 3.2. SSCM-RT Channel Model Simulation

In this paper, the path loss is utilized as a metric to assess the viability of the SSCM-RT model. Its direct path, multipath, and all other paths are all taken into account, and their respective path losses are compared with those of other models. Assume that the high-altitude UAV is stationary and the low-altitude UAV is located at an altitude of 150 m and moves in a circle with a radius of 100 m. The frequency is 40 GHz and the bandwidth is 800 MHz.

The observation of its first-order reflecting rays, Lambert scattering rays are set in the ray tracing model. The UAV is thought to be made of aluminum, which has a real permittivity of 2.15 and a loss tangent of 0.008 in this scenario. The UAV model utilized for the RT part of the simulation is shown in Figure 5.

Except for the direct path, all of the multipaths in the RT part simulation are scattering components. The number of rays is between 15 and 20, as depicted in Figure 6. The result shows symmetry. As a result, the channel has more scattering components and is dominant in this scenario. This further exemplifies the necessity for the ray tracing model. In the study of this UAV channel, the path loss of direct path, multipath, and all paths are compared, respectively.

In the simulation, when using the SSCM-RT hybrid model,  $d_2$  is assumed to be 100 m. The simulation results are shown in Figure 7 and Table 2. Since the measured data for this scenario is challenging, RT simulation results are used as a point of reference.

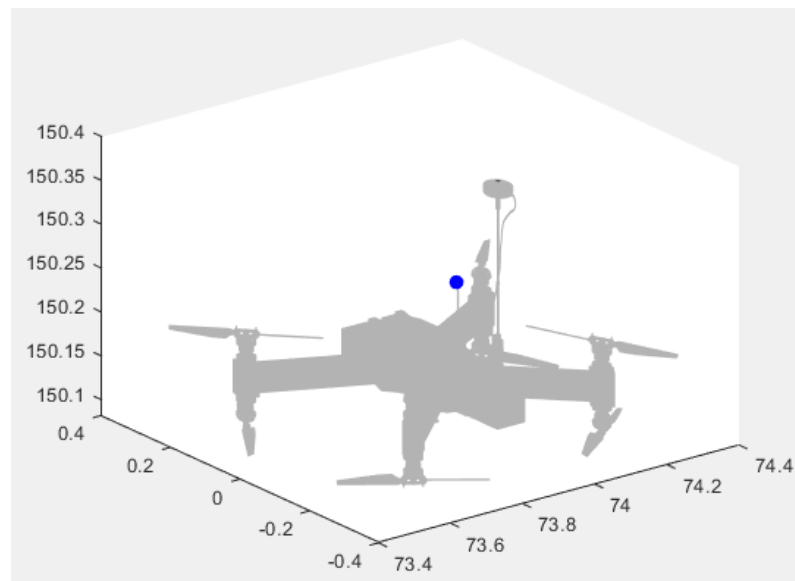


**Figure 5.** The UAV model used for the RT part of the simulation. The blue point is the receiver of antenna.

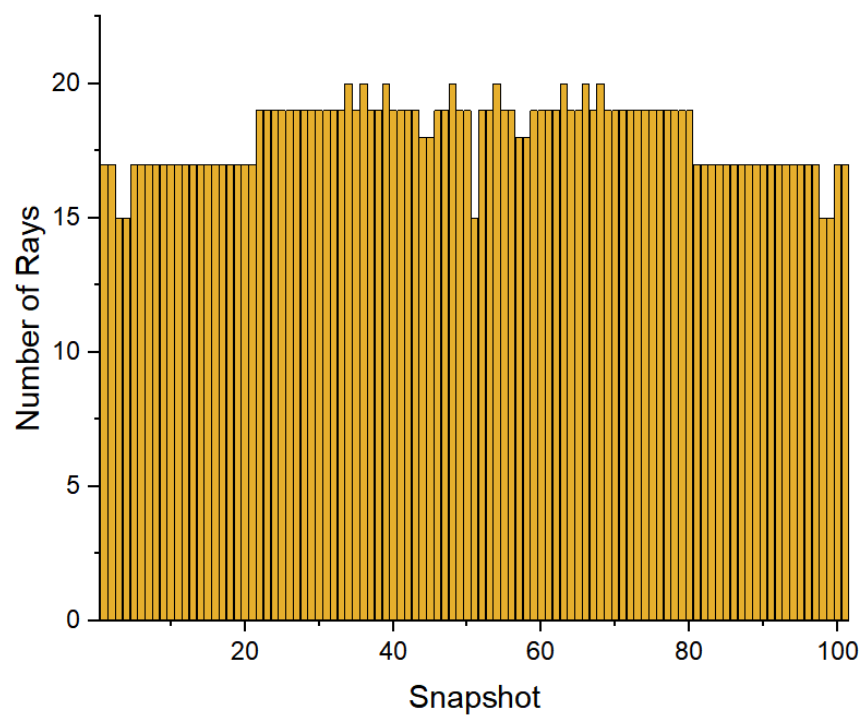
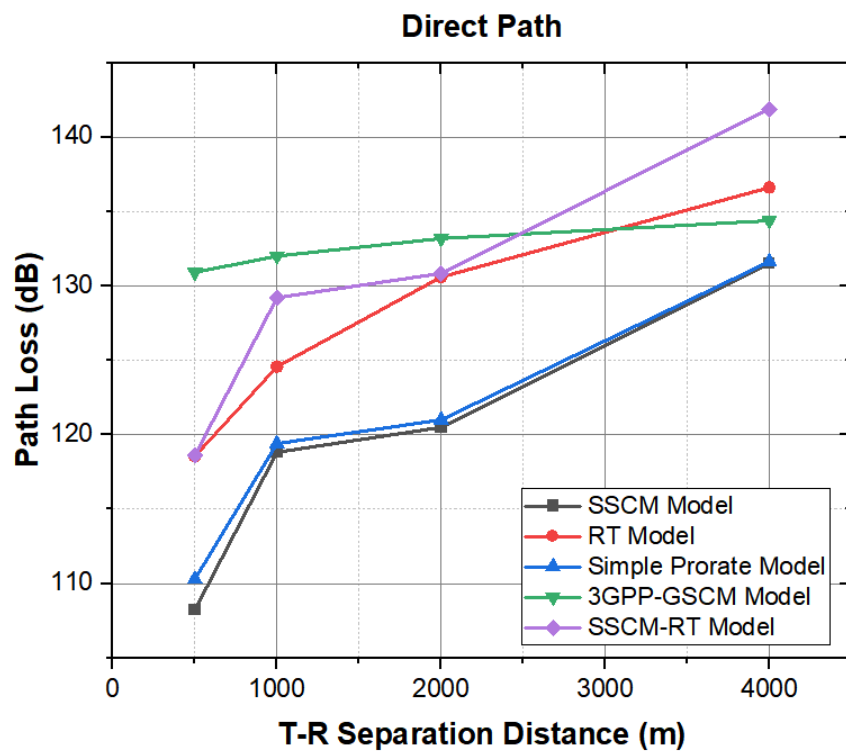
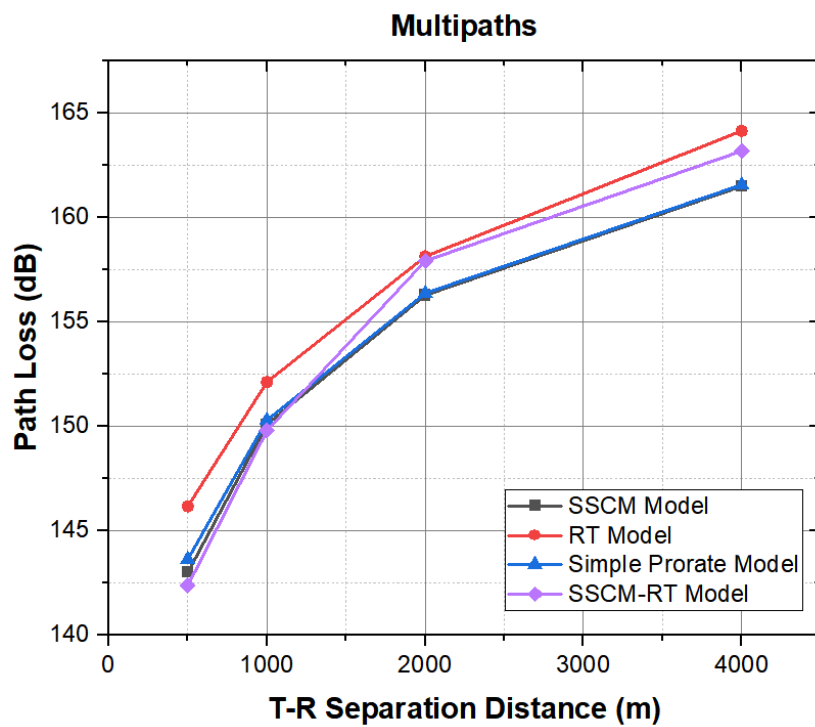


**Figure 6.** Number of rays in motion.



(a)



(b)

Figure 7. Cont.

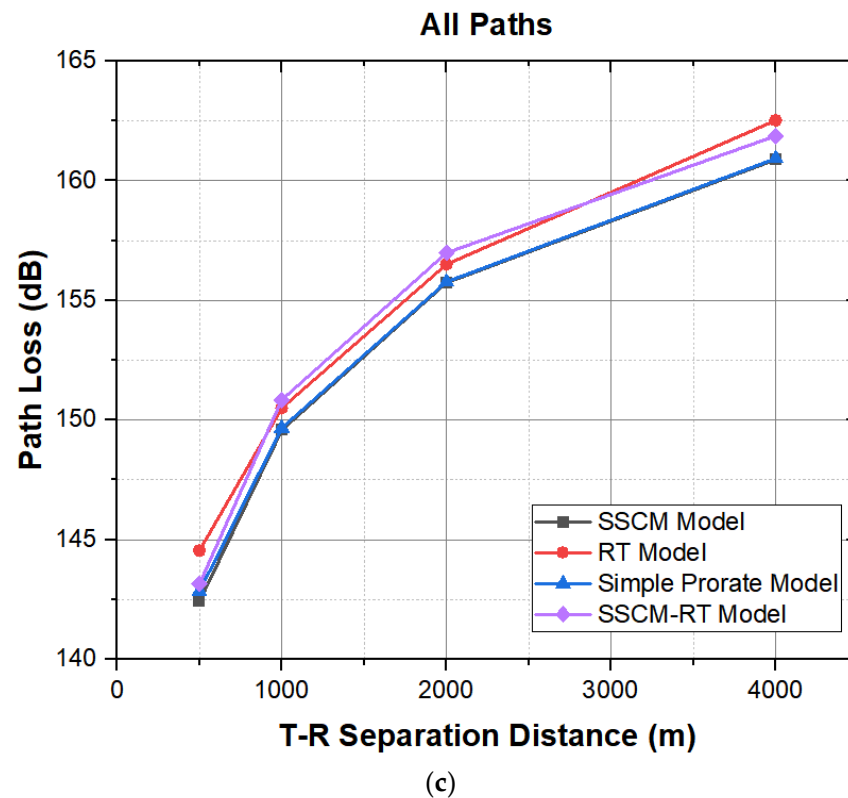


**Figure 7.** Comparison of path loss by using different channel models. (a) direct path; (b) multipaths; (c) all paths.

**Table 2.** Comparison of path loss of different channel models.

Model	Ray Type	T-R 500 m	T-R 1000 m	T-R 2000 m	T-R 4000 m
SSCM Model	Direct Path	108.22 dB	118.82 dB	120.49 dB	131.51 dB
	Multipaths	143.00 dB	150.09 dB	156.27 dB	161.49 dB
	All Paths	142.42 dB	149.57 dB	155.73 dB	160.88 dB
RT Model	Direct Path	118.55 dB	124.57 dB	130.59 dB	136.61 dB
	Multipaths	146.17 dB	152.12 dB	158.12 dB	164.14 dB
	All Paths	144.54 dB	150.50 dB	156.50 dB	162.52 dB
Simple Prorate Model	Direct Path	110.29 dB	119.40 dB	121.00 dB	131.63 dB
	Multipaths	143.64 dB	150.29 dB	156.37 dB	161.56 dB
	All Paths	142.84 dB	149.67 dB	155.77 dB	160.93 dB
3GPP-GSCM Model	Direct Path	130.91 dB	132.00 dB	133.19 dB	134.38 dB
	Direct Path	118.61 dB	129.21 dB	130.84 dB	141.89 dB
SSCM-RT Model	Multipaths	142.38 dB	149.80 dB	157.91 dB	163.17 dB
	All Paths	143.15 dB	150.84 dB	156.98 dB	161.87 dB

When using the results of the ray-tracing-only model as a reference, as shown in Figure 7, the path loss values of the SSCM model are generally smaller due to its error in describing the channel conditions in the near-field. When the T–R distance is smaller, the findings of the SSCM-RT model for the direct path outperform those of the cascaded channel model in reference [15] and the GSCM model from 3GPP TR 38.901 and are closer to the simulation results of the RT model. As the average path loss of the multipath components is utilized as the observation result, the results of the SSCM-RT model for the multipath components are closer to the simulation results of RT when the T–R distance is large. For all paths, the results of the SSCM-RT model can closely match the outcomes of the deterministic model. Therefore, the validity of the SSCM-RT hybrid channel modeling scheme is shown.

According to Equation (8),  $\frac{d_1}{d_2}$  will have an impact on the accuracy of the results of the SSCM-RT hybrid channel modeling. Assuming that the T–R separation distance is 1000 m,  $d_2$  is taken as 20 m, 50 m, 80 m, 100 m, 150 m, and 200 m, corresponding to  $\frac{d_1}{d_2}$  of 49, 19, 11.5, 9, 5.67, and 4, respectively. The ‘RT Distance of SSCM-RT’ of 0 and 1000 m correspond to the results of the spatial statistical channel model and ray tracing model, respectively. A comparison of the path loss for each model is shown in Figure 8.

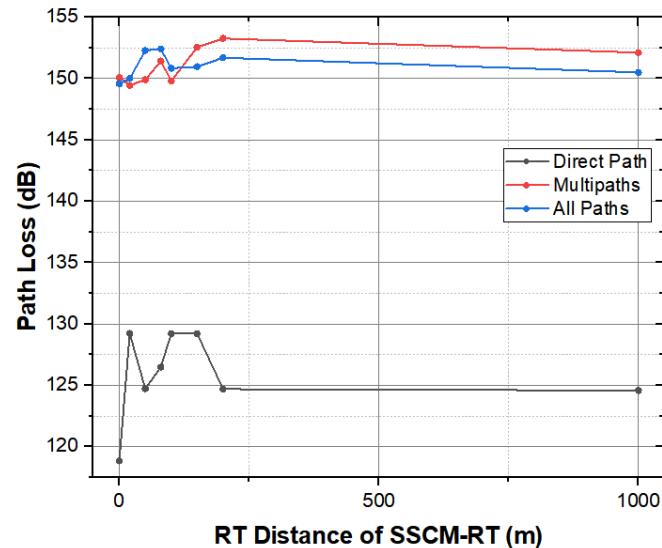


Figure 8. Comparison of path loss in the SSCM-RT channel model with varying  $\frac{d_1}{d_2}$  value.

It can be seen that  $\frac{d_1}{d_2}$  has an impact on the path loss simulation results, but the error value is not large and does not exceed 2 dB when considering the path loss for all paths. In addition, the type and number of rays remain the same as in Figure 6, which further indicates the validity of the SSCM-RT channel model.

#### 4. Spatial Consistency of Dynamic Channels

Two asymmetric motion models are used in this section in order to further confirm the reliability of the SSCM-RT model.

##### 4.1. Spatial Consistency and Motion Models

The measurement of channel properties can be made to fit realistically and exhibit smooth evolution by the introduction of spatial consistency. Figure 9 illustrates the time-varying path loss comparison using SSCM for a linear motion model. As can be observed, spatially correlated shadow fading changes smoothly and corresponds to motion trajectories, but independent shadow fading changes dramatically over a range of around 25 dB. It indicates the significance of channel spatial consistency.

The relative motion relationship can be described using the memory-based, time-based Gauss–Markov model in actual communication scenarios. The Gauss–Markov model is often used in cellular networks and ad hoc networks. The use of the Gauss–Markov model for analysis has practical significance. In the Gauss–Markov model, node movement rate  $v$  and direction  $\theta$  are updated according to a certain time slot interval. It can be expressed as

$$\begin{cases} v_{t+1} = \alpha v_t + (1 - \alpha)\bar{v} + \sqrt{(1 - \alpha^2)}v_n \\ \theta_{t+1} = \alpha \theta_t + (1 - \alpha)\bar{\theta} + \sqrt{(1 - \alpha^2)}\theta_n \end{cases} \quad (9)$$

where  $t$  represents a certain moment and  $t + 1$  represents the next moment. Both  $v$  and  $\theta$  obey the Gaussian distribution  $v_n$  and  $\theta_n$ , and the motion of the whole process depends

on the motion of the previous time, as well as the mean and variance of the Gaussian distribution. The position of the moving object can be expressed as

$$\begin{cases} x_{t+1} = x_t + v_t \cdot t \cdot \cos\theta_t \\ y_{t+1} = y_t + v_t \cdot t \cdot \sin\theta_t \end{cases} \quad (10)$$

Assume that the movement rate of the UAV ranges from 5 to 20 m/s.  $v_t \sim N(10, 0.2)$ ,  $\theta_t \sim N(\pi, 0.2)$ . The number of simulations is set to 200. The trajectory of the two-dimensional Gauss–Markov model is shown in Figure 10.

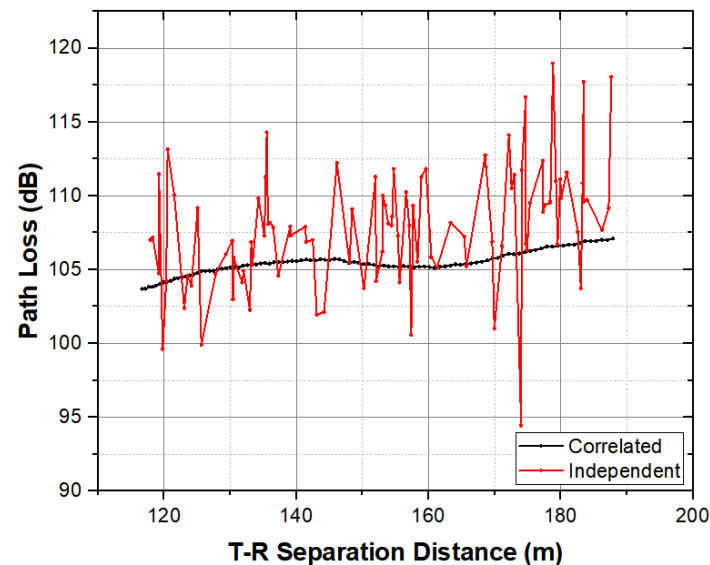


Figure 9. Time varying path loss of linear motion model by using SSCM.

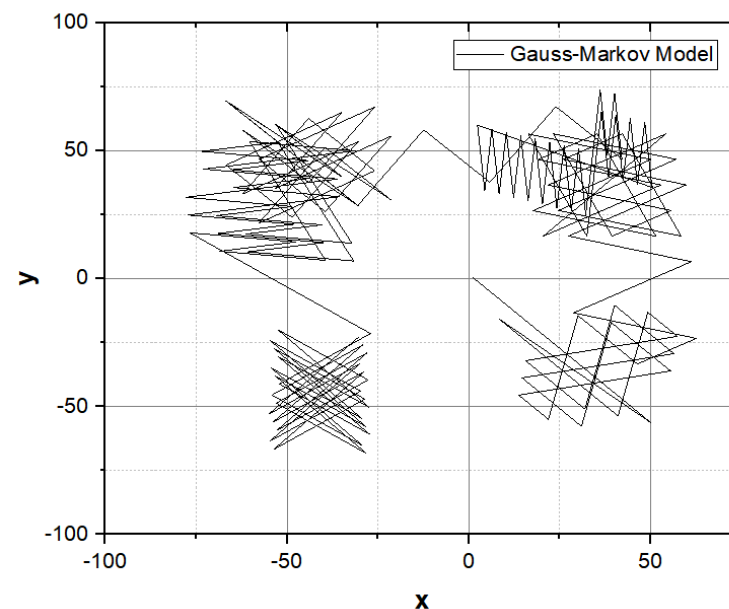


Figure 10. Gauss–Markov model.

The process of the random direction model can be described as follows: Based on the beginning position, the speed, direction, and distance of travel are randomly chosen. After arriving at the destination, the movement's pace, direction, and distance are chosen again. The node can pause and modify the direction of motion while moving in this paper's improved random direction model. The improved random direction model is more accurate in simulating actual motion. Assume that the movement rate ranges from 5 to

20 m/s, each pause time is 0.1 s, and the number of simulations is set to 100. The trajectory of the two-dimensional random direction model is shown in Figure 11.

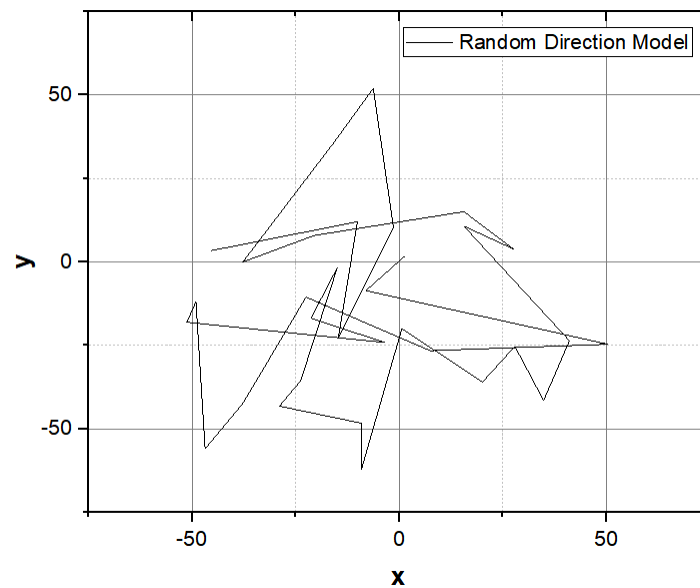


Figure 11. Random direction model.

#### 4.2. SSCM-RT Dynamic Channel Simulation

Figure 12 displays the path loss for the two motion models using the ray tracing model. Accordingly, it can be inferred that the ray tracing model presents spatial consistency in nature. The spatial consistency can be maintained even when the overall path loss is less than 3 dB. Therefore, the introduction of spatial consistency to the linear model, Gauss–Markov model, and random direction model allows for the continuous output of channel state information, which is helpful for the quantitative definition and description of the UAV channel in practical settings.

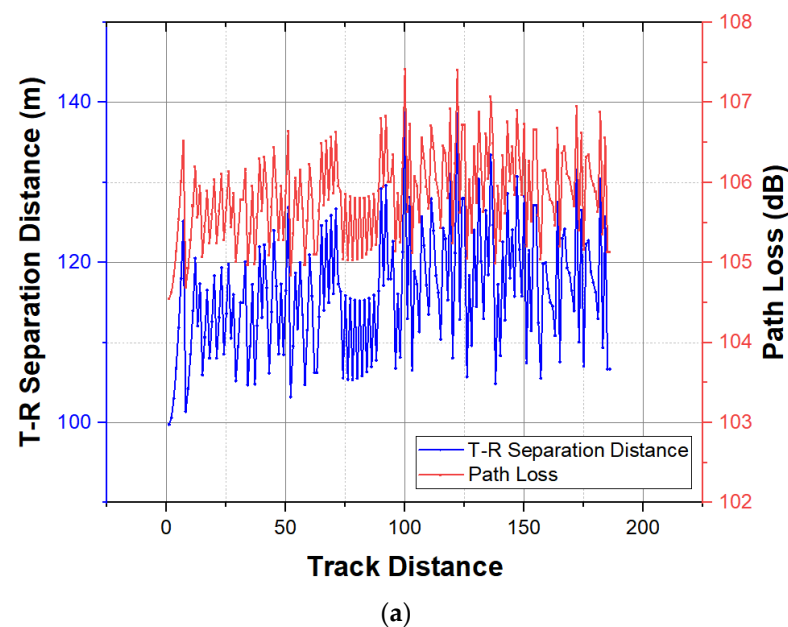
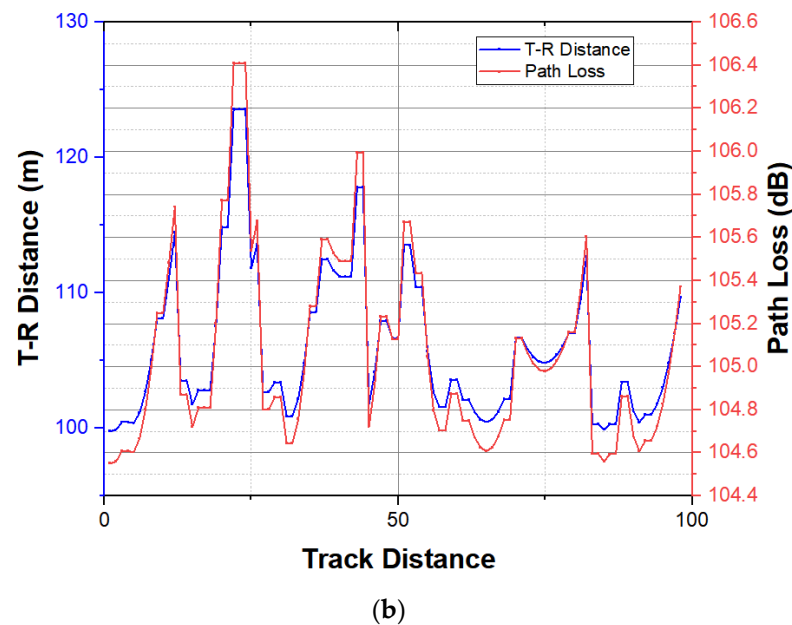
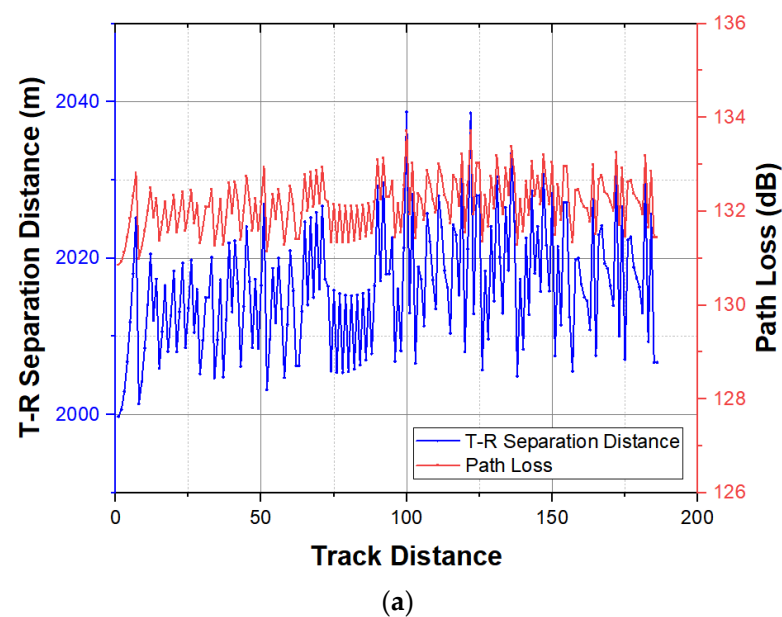


Figure 12. Cont.



**Figure 12.** The path loss of two motion models by using RT model. (a) Gauss–Markov model; (b) random direction model.

Given the above, the spatial consistency is introduced in the statistical channel part of the SSCM-RT model, which is applied to the Gauss–Markov model and random direction model. By characterizing the dynamic channel of the long-distance non-terrestrial network, the reliability of the SSCM-RT model is confirmed from the standpoint of path loss. Assume that  $d_1$  is 1900 m and the initial value of  $d_2$  is 100 m; the value of  $d_2$  varies with the motion process. The path loss under the Gauss–Markov model and random direction model are shown in Figure 13. The simulation findings show that the SSCM-RT hybrid model can maintain spatial consistency during the whole motion process, making it suited for dynamic scenarios with irregular distance changes. Therefore, in comparing the actual relative motion scenarios of a UAV, the SSCM-RT hybrid model has superior channel characterization than the SSCM model.



**Figure 13.** *Cont.*

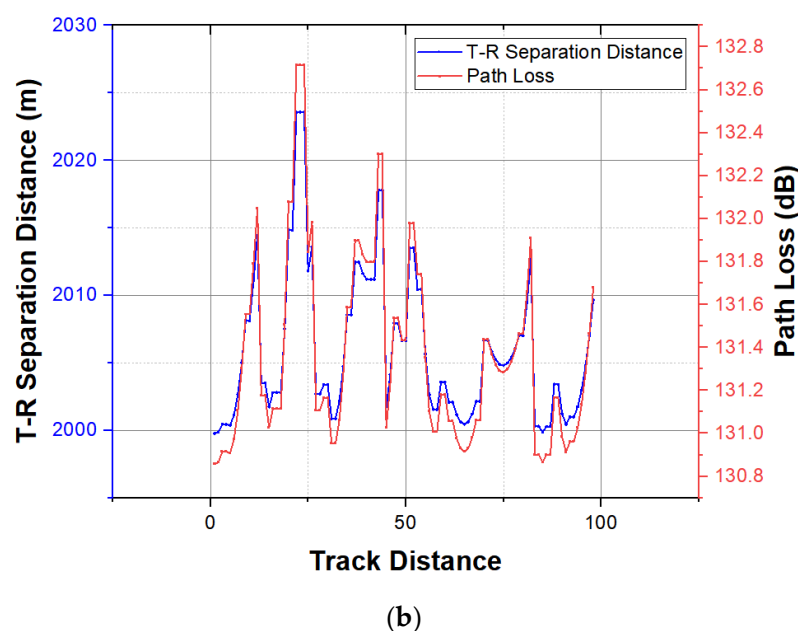


**Figure 13.** The path loss of two motion models by using SSCM-RT model. (a) Gauss–Markov model; (b) random direction model.

## 5. Conclusions

This paper proposes a hybrid spatial statistical ray tracing (SSCM-RT) channel model to cope with long-distance and dynamic communication problems in the non-terrestrial transmission channels of a high altitude, as is the case for UAVs. The spatial statistical channel model provides the parameters to simulate and evaluate the model's performance using frequencies in the range from 28 GHz to 55 GHz. We achieved an error value due to the combined path loss using the SSCM-RT model not exceeding 2 dB. Moreover, the segmentation approach used to model path loss using the hybrid technique reduces the complexity of simulations compared to a full RT model. However, the type and number of rays remain the same. We demonstrated the validity of the SSCM-RT hybrid channel modeling scheme based on path loss given a fixed number of rays in a symmetric scenario. We examine the impact of spatial consistency of the channel model by simulating the relative motion of the UAVs using a Gauss–Markov model and a random direction model. The measurement of channel properties can be made to fit realistically and show a smooth evolution with the introduction of spatial consistency. The SSCM-RT hybrid model with the introduction of spatial consistency is also suitable for dynamic scenarios with irregular distance changes and can maintain spatial consistency during the whole motion process. The reliability of the SSCM-RT hybrid channel modeling scheme is further demonstrated based on the spatial consistency in asymmetric dynamic scenarios.

**Author Contributions:** Methodology, J.Y.; Software, H.X.; Validation, Z.P.; Data curation, Y.Z.; Writing—original draft, H.X.; Writing—review & editing, J.Y. All authors have read and agreed to the published version of the manuscript.

**Funding:** This research received no external funding.

**Data Availability Statement:** No new data were created.

**Conflicts of Interest:** The authors declare no conflict of interest.

## Appendix A

**Table A1.** The Symbols and Descriptions of Channel Parameters.

Parameter	Symbol	Description
T-R Separation Distance (m)	$d_{T-R}$	The separation distance from the transmitter (TX) to the receiver (RX).
Time Delay (absolute propagation time) (ns)	$\tau$	The time it takes for an electromagnetic or optical signal to travel a certain distance in the transmission medium.
Received Power (dBm)	$P_r$	The power RX received.
Path Loss (dB)	$PL$	The loss caused by the propagation of radio waves in space. It is caused by the radiated diffusion of the transmitted power and the propagation characteristics of the channel.
Path Loss Exponent	$n, n_{omni}, n_{dir}, n_{dir-best}$	The path loss exponent ranges from 2 to 6, with 2 representing free space and 6 representing severe obstruction.
Shadow Fading Standard Deviation (dB)	$\sigma, \sigma_{omni}, \sigma_{dir}, \sigma_{dir-best}$	Obstacles attenuate signal power by absorption, reflection, scattering, and diffraction, causing shadow fading. The range is from 5 dB to 12 dB, and the typical value is 8 dB.
TX Ant. HPBW	$AZ_{TX}, EL_{TX}$	An editable parameter denoting the azimuth/elevation half-power-beamwidth (HPBW) of the TX antenna (array) in degrees.
TX Ant. Gain (dBi)	$G_{TX}$	TX antenna gain.
RX Ant. HPBW	$AZ_{RX}, EL_{RX}$	An editable parameter denoting the azimuth/elevation half-power-beamwidth (HPBW) of the RX antenna (array) in degrees.
RX Ant. Gain (dBi)	$G_{RX}$	RX antenna gain.

In the lower corner mark of  $n$  and  $\sigma$ , 'omni' represents omnidirectional, 'dir' represents directional, 'dir - best' represents the direction with the strongest received power.

## References

- Xiao, Z.; Zhu, L.; Liu, Y.; Yi, P.; Zhang, R.; Xia, X.; Schober, R. A Survey on Millimeter-Wave Beamforming Enabled UAV Communications and Networking. *IEEE Commun. Surv. Tutor.* **2022**, *24*, 557–610. [[CrossRef](#)]
- Bai, L.; Huang, Z.; Zhang, X.; Cheng, X. A Non-Stationary 3D Model for 6G Massive MIMO mmWave UAV Channels. *IEEE Trans. Wirel. Commun.* **2021**, *21*, 4325–4339. [[CrossRef](#)]
- You, X.; Wang, C.-X.; Huang, J.; Gao, X.; Zhang, Z.; Wang, M.; Huang, Y.; Zhang, C.; Jiang, Y.; Wang, J.; et al. Towards 6G wireless communication networks: Vision, enabling technologies, and new paradigm shifts. *Sci. China Inf. Sci.* **2020**, *64*, 110301. [[CrossRef](#)]
- Al-Shammari, B.K.J.; Hburi, I.; Idan, H.R.; Khazaaal, H.F. An Overview of mmWave Communications for 5G. In Proceedings of the 2021 International Conference on Communication & Information Technology (ICICT), Basrah, Iraq, 5–6 June 2021; pp. 133–139. [[CrossRef](#)]
- Bian, J.; Wang, C.-X.; Gao, X.; You, X.; Zhang, M. A General 3D Non-Stationary Wireless Channel Model for 5G and Beyond. *IEEE Trans. Wirel. Commun.* **2021**, *20*, 3211–3224. [[CrossRef](#)]
- Wang, J.; Wang, C.-X.; Huang, J.; Wang, H.; Gao, X. A General 3D Space-Time-Frequency Non-Stationary THz Channel Model for 6G Ultra-Massive MIMO Wireless Communication Systems. *IEEE J. Sel. Areas Commun.* **2021**, *39*, 1576–1589. [[CrossRef](#)]
- Khawaja, W.; Guvenc, I.; Matolak, D.W.; Fiebig, U.-C.; Schneckenburger, N. A Survey of Air-to-Ground Propagation Channel Modeling for Unmanned Aerial Vehicles. *IEEE Commun. Surv. Tutor.* **2019**, *21*, 2361–2391. [[CrossRef](#)]
- Liao, C.; Xu, K.; Xie, W.; Xia, X. 3-D massive MIMO channel model for high-speed railway wireless communication. *Radio Sci.* **2020**, *55*, e2020RS007070. [[CrossRef](#)]
- Sun, S.; Rappaport, T.S.; Heath, R.W.; Nix, A.; Rangan, S. Mimo for millimeter-wave wireless communications: Beamforming, spatial multiplexing, or both? *IEEE Commun. Mag.* **2014**, *52*, 110–121. [[CrossRef](#)]
- Zhu, X. Analysis of military application of UAV swarm technology. In Proceedings of the 2020 3rd International Conference on Unmanned Systems (ICUS), Harbin, China, 27–28 November 2020; pp. 1200–1204. [[CrossRef](#)]
- Iqbal, A.; Tham, M.; Wong, Y.J.; Al-Habashna, A.; Wainer, G.; Zhu, Y.X.; Dagiuklas, T. Empowering Non-Terrestrial Networks with Artificial Intelligence: A Survey. *IEEE Access* **2023**, *11*, 100986–101006. [[CrossRef](#)]
- Mahboob, S.; Liu, L. Revolutionizing Future Connectivity: A Contemporary Survey on AI-empowered Satellite-based Non-Terrestrial Networks in 6G. *arXiv* **2023**. [[CrossRef](#)]

13. Traspadini, A.; Giordani, M.; Zorzi, M. UAV/HAP-Assisted Vehicular Edge Computing in 6G: Where and What to Offload? In Proceedings of the 2022 Joint European Conference on Networks and Communications & 6G Summit (EuCNC/6G Summit), Grenoble, France, 7–10 June 2022; pp. 178–183. [\[CrossRef\]](#)
14. Chen, Y.; Li, Y.; Han, C.; Yu, Z.; Wang, G. Channel Measurement and Ray-Tracing-Statistical Hybrid Modeling for Low-Terahertz Indoor Communications. *IEEE Trans. Commun.* **2021**, *20*, 8163–8176. [\[CrossRef\]](#)
15. Luo, W.; Ma, Y.; Shao, X.; Xu, L.; Nan, X. A hybrid near and far-field channel model based on large-scale reconfigurable smart surfaces. *J. Electron. Inf. Technol.* **2022**, *44*, 3866–3873. [\[CrossRef\]](#)
16. Khuwaja, A.A.; Chen, Y.; Zhao, N.; Alouini, M.-S.; Dobbins, P. A Survey of Channel Modeling for UAV Communications. *IEEE Commun. Surv. Tutor.* **2018**, *20*, 2804–2821. [\[CrossRef\]](#)
17. Yang, J.; Li, H.; Xu, Z. Analysis of channel characteristics between satellite and space station in terahertz band based on ray tracing. *Radio Sci.* **2021**, *56*, e2021RS007290. [\[CrossRef\]](#)
18. Yang, J.; Yuan, L. Analysis of channel characteristics for inter-satellite terahertz communication based on Lambertian model. *J. Signal Process.* **2022**, *38*, 232–240. [\[CrossRef\]](#)
19. Rappaport, T.S. *Wireless Communications: Principles and Practice*; Prentice Hall PTR: Hoboken, NJ, USA, 1996.
20. Chetlur, V.V.; Dhillon, H.S. Downlink Coverage Analysis for a Finite 3-D Wireless Network of Unmanned Aerial Vehicles. *IEEE Trans. Commun.* **2017**, *65*, 4543–4558. [\[CrossRef\]](#)
21. Mou, M.A.; Mowla, M.M.; Aftabi Momo, S.H. Statistical Channel Model at mmWave Band Inside High Speed Water Vehicle. In Proceedings of the 2019 3rd International Conference on Electrical, Computer & Telecommunication Engineering (ICECTE), Rajshahi, Bangladesh, 26–28 December 2019; pp. 109–112. [\[CrossRef\]](#)
22. Teixeira, E.; Sousa, S.; Velez, F.J.; Peha, J.M. Impact of the propagation model on the capacity in small-cell networks: Comparison between the UHF/SHF and the millimeter wavebands. *Radio Sci.* **2021**, *56*, e2020RS007150. [\[CrossRef\]](#)
23. Jawhly, T.; Chandra Tiwari, R. Loss exponent modeling for the hilly forested region in the VHF band III. *Radio Sci.* **2021**, *56*, e2020RS007201. [\[CrossRef\]](#)
24. Sun, S.; MacCartney, G.R.; Rappaport, T.S. A novel millimeter-wave channel simulator and applications for 5G wireless communications. In Proceedings of the 2017 IEEE International Conference on Communications (ICC), Paris, France, 21–25 May 2017; pp. 1–7. [\[CrossRef\]](#)

**Disclaimer/Publisher’s Note:** The statements, opinions and data contained in all publications are solely those of the individual author(s) and contributor(s) and not of MDPI and/or the editor(s). MDPI and/or the editor(s) disclaim responsibility for any injury to people or property resulting from any ideas, methods, instructions or products referred to in the content.